Title

Applicators for Magnetic Resonance–Guided Ultrasonic Ablation of Benign Prostatic Hyperplasia

Journal

Investigative Radiology, 48(6)

ISSN

0020-9996

Authors

Sommer, Graham
Pauly, Kim Butts
Holbrook, Andrew
et al.

Publication Date

2013-06-01

DOI

10.1097/rli.0b013e31827fe91e

Peer reviewed

Published in final edited form as:
Invest Radiol. 2013 June ; 48(6): 387–394. doi:10.1097/RLI.0b013e31827fe91e.

Applicators for MR-Guided Ultrasonic Ablation of BPH

Graham Sommer, MD[1], **Kim Butts Pauly, PhD**[1], **Andrew Holbrook, PhD**[1], **Juan Plata, MS**[1], **Bruce Daniel, MD**[1], **Donna Bouley, PhD, DVM**[2], **Harcharan Gill, MD**[3], **Punit Prakash, MS**[4], **Vasant Salgaonkar, MS**[4], **Peter Jones, MS**[4], and **Chris Diederich, PhD**[4]

[1]Department of Radiology, Stanford University School of Medicine

[2]Department of Comparative Medicine, Stanford University School of Medicine

[3]Department of Urology, Stanford University School of Medicine

[4]UCSF Department of Radiation Oncology

Abstract

Objectives—To evaluate in a canine model, applicators designed for ablation of human benign prostatic hyperplasia (BPH) *in vivo* under MRI guidance, including magnetic resonance thermal imaging (MRTI). To determine the ability of MRI techniques to visualize ablative changes in prostate, and to evaluate the acute and longer term histologic appearances of prostate tissue ablated during these studies.

Materials and Methods—A MRI-compatible transurethral device incorporating a tubular transducer array with dual 120 sectors was employed to ablate canine prostate tissue *in vivo*, in zones similar to regions of human BPH (enlarged transition zones (TZ)). MRTI was used for monitoring of ablation in a 3T environment, and post-ablation MRI's were performed to determine visibility of ablated regions. Three canine prostates were ablated in acute studies, and 2 animals were rescanned prior to sacrifice at 31 days post ablation. Acute and chronic appearances of ablated prostate tissue were evaluated histologically, and correlated with the MRTI and post ablation MRI scans.

Results—It was possible to ablate regions similar in size to enlarged TZ in human BPH in 5 to 15 minutes. Regions of acute ablation showed a central “heat fixed” region surrounded by a region of more obvious necrosis with complete disruption of tissue architecture. After 31 days, ablated regions demonstrated complete apparent resorption of ablated tissue with formation of cystic regions containing fluid. The inherent cooling of the urethra using the technique resulted in complete urethral preservation in all cases.

Conclusions—Prostatic ablation of zones of size and shape corresponding to human BPH is possible using appropriate transurethral applicators using MRTI, and ablated tissue may be depicted clearly in contrast-enhanced MR images. The ability accurately to monitor prostate tissue heating, the apparent resorption of ablated regions over one month, and the inherent urethral preservation suggest the MR guided technques described are highly promising for the *in vivo* ablation of symptomatic human BPH.

Introduction

It has been noted that, in spite of its small normal size and weight (about 20 grams in young adult males), the prostate is affected with a remarkable prevalence of significant pathologies in men's later years[1,2]. In addition to prostate cancer, which has the highest prevalence of any male nondermatologic malignancy, benign prostatic hyperplasia (BPH) also has a remarkably high prevalence, increasing with age. A wide range of terminologies have been used to describe a symptom complex including diminished urinary flow rates, and associated with significant BPH, with the current favored descriptive being “lower urinary tract symptoms” (LUTS)[3]. LUTS comprises a range of symptomology that can be graded by standard scoring symptoms based on specific patient signs and symptoms. The significance of BPH and the clinical importance of LUTS may be inferred by the facts that by age 60, the prevalence of notable BPH is greater than 50%, and the prevalence of moderate to severe LUTS in men aged 60 to 69 years is in the range of thirty to forty percent[3-5].

It is instructive to consider the lobar anatomy of the prostate described by McNeal[1,6], to understand the characteristic pathologic changes associated with BPH. A range of appearances have been described for BPH, and various terminologies have been used to describe these variants. Basically, however, BPH involves glandular and stromal hyperplasia in two prostatic zones in the McNeal classification that are in close proximity to the prostatic urethra. In a substantial majority of patients, enlargement of the transition zone (TZ) lobes, located anterolateral to the prostatic urethra, dominates the structural changes leading to urethral obstruction and obstructive symptomology (Figure 1 A and B). As shown, the urethra can be greatly compressed between the enlarged TZ lobes, and it can easily be seen that such compression will tend to narrow the prostatic urethra, leading to obstruction of urinary flow. The second McNeal prostatic region significantly involved with BPH is the periurethral zone containing periurethral glands (PUG). Enlargement of the PUG in the periurethral zone leads to a pattern of BPH characterized by retrourethral or “median lobe” enlargement. While combined lobar enlargement is often involved in detailed descriptions of BPH[3], the pathologic pattern and obstructive effects are largely dominated by the enlarged TZ lobes, and “median lobe” enlargement is dominant in only about 10% of cases.

While medical therapy for BPH has become increasingly utilized, surgical options including transurethral resection of the prostate (TURP), and open prostatectomy are still very commonly used to treat symptomatic BPH. The volume of surgeries in the US for BPH is currently 3 to 4 times that of radical prostatectomies for prostate cancer[3,4]. Significant patient morbidity has been associated with standard surgical procedures for BPH. While reported complication rates are variable, TURP, for instance, is often associated with significant hemorrhage, and carries a small risk of postoperative urinary incontinence and impotence. The search for a simpler technique for BPH ablation with less associated morbidity has lead to the development of a range of minimally invasive techniques to treat symptomatic BPH. The goal of such techniques is generally the ablation or reduction in size of the enlarged TZ lobes compressing the prostatic urethra, with dominant “median lobe” enlargement considered a contraindication to such approaches.

The purpose of the studies reported here is the description of a system for prostatic ablation using a MRI-compatible transurethral applicator designed specifically for minimally invasive treatment of human BPH through ablation of the enlarged bilateral TZ lobes, with initial *in vivo* evaluation in studies of enlarged canine prostates. It may be expected that ablation of TZ tissue compressing the prostatic urethra in the human male may be effective in alleviating urethral compression and LUTS. In prior studies, various types of MRI-compatible transurethral applicators incorporating cylindrical, planar and focused piezoelectrics have been described[7-14], and all have been found capable of using MRTI (magnetic resonance thermal imaging) guidance for accurate targeting and ablation of canine prostate tissue *in vivo*. Such studies have clearly indicated the potential of using MRI to plan, monitor and evaluate tissue changes during and after prostatic ablation with such applicators, and indicate promise for controlled ablation of targeted prostate tissues with minimal damage to sensitive adjacent structures, and minimal side effects. Recently[15,16], the feasibility of ablation of human prostatic tissues using MRI-compatible transurethral applicators incorporating planar piezoelectrics and controlled rotation has been demonstrated, furthering the preliminary translation of these MRI-guided transurethral technologies into the clinical environment.

Materials and Methods

Transurethral ultrasound applicators consisting of multi-sectored tubular transducer arrays were devised to sonicate and ablate the anterolateral portions of the prostate gland between the bladder neck and veromantum, the region corresponding to the enlarged TZ lobes in human BPH (Figure 1). The cylindrical array elements consisted of 7 MHz, 10 mm long × 3.5 mm OD, dual 120° sectors with 30° anterior inactive zones. Such applicators can directly insonate and heat conformal contiguous regions corresponding to the hyperplastic human TZ lobes, providing precise control of ablation within relatively short treatment times. Power to the applicators was supplied using a multichannel RF amplifier (Advanced Surgical Systems, Tucson, Arizona) located outside the MR suite. In-line low-pass filters were employed at the penetration panel to reduce device noise and prevent possible image degradation. The arrays were positioned on the distal end of a flexible catheter within an expandable cooling balloon (Figure 2), positioned within the prostatic urethra during the ablative procedure. A 5 cc bladder balloon on the distal end of the applicator was employed for device retention during the procedure. Rapid MR imaging sequences, including spoiled gradient recalled (SPGR) and rapid T2 weighted sequences such as single-shot fast spin echo (SSFSE) were used repeatedly to monitor device positioning and assure good placement within the prostate. Transurethral devices were positioned within the gland, and secured in place by filling the small retention balloon with a 2% solution of gadolinium contrast agent to keep the device anchored in place. The transurethral devices were then rotated while in place to adjust targeting along a radial axis from the urethra, so as to insonate along 2 desired anterolateral paths.

The most critical role of MRI is in monitoring of prostate and periprostatic heating during the ablative process, and real-time proton resonant frequency (PRF) imaging was performed during the ablative procedure to create and display real time magnetic resonance thermal imaging (MRTI). The basic principle allowing the creation of PRF thermal images is the fact

that the phase change φ, detected using gradient recalled images, can directly be used to create images that depict temperature in prostate tissues. It can be shown that the relationship between the temperature change in tissues ΔT can be expressed as:

$$\Delta T = \frac{\phi - \phi_0}{\gamma \alpha B\, TE}$$

where α is the temperature change coefficient -.01 ppm/°C for aqueous tissues, α is the gyromagnetic ratio for water protons, B is the main magnetic field strength, TE is the echo time, and φ_0 is the initial phase before heating begins. Since body temperature is known, the above equation can be used to create phase-sensitive gradient echo images that directly encode local tissue temperature. Such images can be rapidly acquired and displayed at real time rates as overlays on images displaying anatomic detail.

Our MRI studies in 5 canine prostates were performed in a Signa (General Electric Healthcare, Schenectady New York) 3 T scanner with body transmit coil and high SNR endorectal (ER) coils, incorporating a cooling jacket using circulating water. Multislice gradient recalled MR images were acquired at 3 levels, having slice thickness of 5 mm and in-plane resolution of 0.625 by 1.25 mm, typically every 15 seconds. Baseline images needed for phase reference were acquired before heating, and MR thermal imaging (MRTI) continued throughout the application of ultrasound energy and during tissue cooling. To correct for baseline drift, the apparent temperature rise in a region of interest (ROI) in adipose tissue adjacent to the prostate was measured, and the values in fat subtracted from data from the entire image. Adding the animal's core temperature to all pixels in the temperature map, the temperature throughout the prostate was displayed in MRTI encoding the temperature range of interest in the range of 47°C to 60°C in a color display. The details of the MRTI computation and display are discussed in much more detail elsewhere. [26,28,29] Tracking coils in the transurethral applicator were used to allow rapid accurate applicator localization, and a software real-time environment termed RThawk (Heartvista Inc., Los Altos CA) allowed for the setting up of “control points” in real-time MRI to allow MRTI feedback control of ultrasonic and automated control of the ablative process[29,35]. Figure 3 illustrates the principles of treatment planning with this approach; targeted regions for ablation were outlined, and control points set up, which provide interactive feedback to the ablation procedure via modulation of power output to the piezoelectric ultrasound elements in the applicator. Post ablation scans were performed including contrast enhanced (CE), T2 weighted (T2W) and diffusion weighted imaging (DWI). Figure 4 illustrates MR imaging of the ablative procedure in an acute study of one canine prostate. Maximum temperature mapping of the canine prostate, and total thermal dose delivery are illustrated in the MRTI, and nonperfusion of the bilateral ablated regions of prostate is documented in a contrast enhanced T1-weighted image at the same level in the gland. Following each study, MRTI monitoring during the exam and post ablation scans were correlated with histologic features of the resected prostates sectioned in the same axial planes as the MRTI and post ablation scans. In 3 studies, there was immediate animal sacrifice after MRI guided ablation (acute study), and in 2 animals, the animals were re-scanned and then sacrificed 31 days after the

ablative procedures (“chronic” study). Freshly resected canine prostates were stained with the vital stain TTC (triphenyltetrazolium chloride) as well as standard H and E and Trichrome stains on formalin-fixed tissues. The technical details of these studies are described in much more detail elsewhere [9,10,12,13,18,21,25,30-34]

Results

The histologic appearances in all cases of acute prostate thermal injury had similar appearances; a representative case of the histologic appearances of acutely ablated prostatic tissue is shown in Figure 5. As can be seen in the MRTI of Figure 5A, the central portion of the ablated regions undergo the greatest elevation in temperature, with temperatures falling off to about 50°C at the margins of the ablated regions. Interestingly, the acutely ablated regions of prostate tissue do not have a homogeneous appearance, but 2 rather distinct regions corresponding to the central region rapidly heated to the highest temperatures, and a peripheral region subjected to lower and more slowly evolving temperature rise. On H&E staining, (Figure 5A) the central regions, heated rapidly to high temperature appeared relatively normal giving an appearance previously described [36]as “heat fixed” (HF), surrounded by a distinct region (5B) of transition to normal prostate, or transition zone (TZ). It became clear at higher power (figures 5C and D), however, that while the glands within the HF region maintained normal histoarchitecture, epithelial cells had an increased affinity for eosin staining, and most cell nuclei appeared smaller and more hyperchromatic than normal. Similar nuclear changes were noted in the interstitial vascular endothelium and smooth muscle cell nuclei. Peripheral to the HF region within zones of ablation, the second distinct region (TZ) was characterized by dramatic disruption of normal histoarchitecture (figure 5B and D). Fragmentation of glands in these areas was severe, and most glands were devoid of attached epithelial cells and had lumina filled with sloughed epithelial cells and granular eosinophilic debris. The heat fixed and transition zones corresponded to tissue regions demonstrating lack of enhancement on contrast enhanced MR imaging and complete lack of staining with TTC.

In the 2 cases in which the ablated region was evaluated at MR imaging and histologically at 31 days, there was complete apparent resorption of ablated tissue with formation of fluid-filled cystic cavities. An example of this appearance is seen in Figure 6 in which the ablated region is seen in the contrast enhanced MRI as a dark nonenhancing region (figure 6A) and cystic tissues defect in the trichrome stained histologic section at this level (6B). Complete preservation of the prostatic urethra during the ablative process was noted in all cases, and is seen both in the trichrome image (6B) and the T2 weighted images (6C and D) from this study.

Discussion

The immediate, or acute changes in prostate tissue immediately following thermal ablation, are of interest, since it is important to confirm true tissue death at the histologic level. The chronic or longer term fate of such ablated tissue is also of note, since it might be possible for ablated tissue to remain in place in a necrotic state, be resorbed by the body, sloughed from the body, or perhaps in part undergo regeneration. All acute studies showed

nonperfused regions after ablation, in contrast-enhanced MR images (figure 4C) which corresponded well to regions of heat-fixed (HF) tissue which appeared relatively similar to normal prostate tissue, and a transition region (TZ) which showed a disorganized appearance more typical of coagulative necrosis (Figure 5). In the cases in which the ablated region of the prostate was evaluated at MR imaging, particularly in post-ablation CE images, and histologically at 31 days (Figure 6), there was complete apparent resorption of ablated tissue with formation of fluid-filled cystic cavities. In prior studies of HF lesions in human liver, the HF appearance persisted over as long as 14 months in studies by Coad et al. [36], so the finding of apparent resorption of ablated HF prostatic tissue over 31 days provides an indication that tissue resorption of thermal lesions may occur in prostate, but not human liver. Prior *in vivo* work by Kincaide[37] and Gelet[38] has supported the concept that chronic thermal lesions in prostatic tissue are resorbed, leaving cystic spaces.

The studies of the transurethral applicator designed for ablation of the enlarged TZ in human BPH have shown capability for the ablation of well-defined regions of prostate tissue anterolateral to the urethra, similar in appearance to TZ lobes in human BPH. It can be seen in Figures 5 and 6, however, that the pattern of BPH in the human differs somewhat from that seen in the canine prostate. In the older canine prostate involved with extensive BPH, cystic change can be seen throughout the entire gland in both figures. In humans, while there is some involvement of all prostatic lobes with BPH, including the peripheral zone (PZ), the enlarged bilateral TZ lobes clearly dominate the pathologic appearance as seen in MR images (Figure 7). Thus the studies demonstrated the ability to guide, monitor and accurately image regions of the canine prostate corresponding the locations of enlarged TZ in humans, but did not represent an attempt to ablate all BPH present throughout the enlarged canine prostate glands.

The objective of the particular transurethral applicator employed was the ablation of regions similar in size and location to enlarged human TZ lobes without significant damage to adjacent structures. The observation that the acutely ablated regions of canine prostate were apparently resorbed at about one month appears encouraging for the clinical utility of the technique for BPH ablation, since such resorption should decrease pressure on the prostatic urethra significantly. Additionally, the complete preservation of the urethra made possible by the inherent cooling due to circulating water in the applicator also seems very desirable, since an intact and decompressed prostatic urethra might also be expected to facilitate greater urinary flow rates and perhaps relieve obstructive symptomology in patients afflicted with BPH and LUTS.

It is, of course, not possible to determine the extent to which clinical LUTS might be relieved by the replacement of hyperplastic TZ tissue in the human by cystic spaces, but some informed conjecture seems possible. Comparison of the results our studies to those of clinical transurethral needle ablation (TUNA) studies seems reasonable, since the objective of both the approach described in our studies, and studies of clinical BPH ablation with TUNA is the destruction of hyperplastic TZ tissue compressing the prostatic urethra. While current TUNA techniques cannot be monitored with MRI, the appearances of regions of the prostate ablated have been documented with post-treatment MRI studies[39]. In these studies, irregularly shaped regions of nonperfusion were observed, apparently corresponding to

zones of necrosis with the portions of the hyperplastic TZ tissue, in patients with decreased obstructive symptomology following the ablative procedure. TZ ablation generally was documented in only a portion of the enlarged TZ of patients studied in this manner, and clear-cut evolution of the regions into cystic spaces was not documented histologically. Nonetheless, significant improvement in obstructive symptoms and maximal urinary flow rates have been documented in clinical studies of the TUNA technique. Since accurate MRTI monitoring of prostatic ablation, not possible with TUNA, is possible with MRI-compatible transurethral applicators, it seems possible and perhaps likely that more accurate and complete bilateral TZ ablation may be possible this approach. As seen in Figure 7, the size and symmetry of enlarged TZ lobes in the human male are quite variable from patient to patient, and only a technique in which thermal tissue ablation can be monitored would appear capable of safely producing maximal ablation of hyperplastic TZ tissue lobes. Additionally a recent case report of MRI-guided cryotherapeutic ablation of TZ lobes has indicated this technique may also be capable of significant improvement in obstructive symptoms and urinary flow rates[40], providing further substantiation for the general efficacy of the MR-guided approach to TZ ablation in BPH.

It is interesting to compare the relative potential for MRI-guided transurethral ultrasonic ablation techniques to the problems of clinically significant BPH and to the focal ablation of prostate cancer. There is currently intense interest in the concept of focal ablation of the largest zone of cancer, or "index lesion" [41,42]within the prostate gland, particularly given the questionable benefit of standard treatments including radical prostatectomy[43,44]. MRI-guided ablation of such index lesions faces some daunting challenges, including the fact that current MRI techniques are not capable of very accurate depiction of the distribution of prostate cancer within the gland. Prospective studies comparing preoperative MR localization of prostate cancer to step-section histologic analysis of prostatectomy specimens have yielded AUC (area under ROC curve) values typically between .58 and .70[45,46], indicating a poor ability of currently available techniques to depict human prostate cancer *in vivo*. The enlarged TZ lobes, on the other hand (Figure 7), are clearly depicted even in conventional T2 weighted MRI, making targeting straightforward using MRI guidance. A further challenge for focal prostate cancer ablation relates to its location generally in the posterior regions (PZ) of the prostate gland. Some of these problems can be illustrated with reference to figure 7, which provides indication of the close proximity of the posterior portions of the gland to critical structures to which damage must be avoided, or at least minimized. In addition to the critical anterior rectal wall, the posterolateral aspects of the prostate gland are in intimate contact with the bilateral neurovascular bundles (NVB), at least one of which must be preserved if patient potency is to be maintained. Seventy percent of prostate cancers arise from the posterior peripheral zone (PZ) of the prostate[47], adjacent to the rectum and bilateral NVB, and a substantial majority of index prostate cancer lesions will be posteriorly located in very close proximity to these very sensitive structures. The ability of transurethral applicators focally to ablate index cancer lesions can be expected to be limited if damage to these sensitive structures is to be avoided. Likely technical advantages for BPH ablation compared to focal cancer ablation then, include consistent MRI visibility of the TZ regions to be ablated, a "buffer zone" of posterior prostate tissue (PZ) making damage to the rectum and NVB unlikely, and the fact that ablation of the entirety of

the enlarged TZ lobes is not required for improvement of LUTS, but ablation of the entire index lesion seems highly desirable for focal treatment of prostate cancer.

The fact that a great many techniques for medical and surgical treatment of BPH exist attests to the fact that no single technique is effective and appropriate in all cases. While medical treatments are effective and have decreased the need for operative approaches, there is substantial expense and significant side effects associated with these techniques, which must be continued indefinitely[4]. There seems no question that transurethral resection (TURP) remains the surgical gold standard for significant and durable improvement in obstructive symptomology and maximal urinary flow rates in individuals afflicted with BPH[4]. On the other hand, a wide variety of minimally invasive techniques have been shown capable of creating fewer of the undesirable effects of TURP, while providing somewhat less substantial and less durable improvements in LUTS symptoms. The list of minimally invasive approaches that have been assessed is long and includes TUNA, transurethral microwave therapy, laser techniques, transurethral incision, transrectal HIFU, transurethral vaporization techniques and even the use of hot water (water-induced thermotherapy)[4].

The use of transrectal HIFU for clinical BPH ablation necessitates some comment due to its superficial similarity to transurethral ultrasonic prostatic ablation. Transrectal HIFU has been assessed in many studies of clinical BPH, with recent analysis indicating that significant improvements in urinary flow rates and symptomology is not substantial, and certainly not durable, with 43.8% of patients requiring TURP for relief of symptoms within 4 years following the HIFU procedure[48]. The transrectal HIFU technique does not seem appropriate for relief of obstructive symptoms; in fact urinary retention in patients in patients undergoing transrectal HIFU for cancer treatment is such a common problem that the procedure is generally accompanied by surgical TURP [49] at present. Transrectal HIFU is a very different technique than transurethral TZ ablation; it is essentially an unmonitored technique, with no indication of tissue heating available during the procedure. During the technique, an effort is made to build up a series of small ablated regions within the entire prostate gland, with no ability specifically to target the enlarged TZ lobes and spare the urethra. The result of the HIFU procedure is inevitably the creation of a large region of coagulative necrosis within the prostate with destruction of the prostatic urethra. The technique contrasts vividly with the controlled ablation of bilateral TZ lobes achievable with MRI-guided transrectal HIFU, ultimately resulting in the creation of cystic spaces, and urethral sparing. There is every reason to expect superior results for MRI-guided transurethral ultrasonic ablation compared to transrectal HIFU approaches.

The results of the studies reported herein give significant promise for the clinical treatment of BPH using transurethral applicators. The ability to plan, guide and evaluate the ablative process with MRI seems crucial for accurate ablation of enlarged TZ lobes associated with BPH and the inherent ability to spare the prostatic urethra also seems highly desirable for alleviation of obstructive symptoms. While it is not clear whether the replacement of enlarged TZ lobes with fluid-filled cystic spaces will provide adequate relief of BPH symptoms, comparison to results of clinical studies of other technologies including TUNA indicate improvement in clinical symptoms can be expected to be substantial. Such fluid-filled spaces could be readily drained by transrectal needle aspiration in any case, possibly

further enhancing relief of BPH symptoms and improvement of urinary flow rates. From a number of perspectives, therefore, transurethral ablation of TZ hyperplasia in BPH appears to have the potential to be a nearly ideal technique for the treatment of clinically significant BPH.

Acknowledgments

The work described in this paper was supported by grants R01 CA11198, R01 CA122276, R21 CA137472, P01 CA159992, and R01 CA121163 from the NIH.

References

1. McNeal JE. Normal and pathologic anatomy of prostate. Urology. 1981; 17(Suppl 3):11–16. [PubMed: 6163241]
2. McNeal JE. Origin and evolution of benign prostatic enlargement. Invest Urol. 1978; 15(4):340–345. [PubMed: 75197]
3. Wasserman NF. Benign prostatic hyperplasia: a review and ultrasound classification. Radiol Clin North Am. 2006; 44(5):689–710. viii. [PubMed: 17030221]
4. McDougal, WS.; Wein, AJ.; Kavoussi, LR., et al. Campbell-Walsh Urology 10th Edition Review E-Book. A Saunders Title; 2011. p. 704
5. McNeal JE. Anatomy of the prostate and morphogenesis of BPH. Prog Clin Biol Res. 1984; 145:27–53. [PubMed: 6201879]
6. McNeal JE. The prostate and prostatic urethra: a morphologic synthesis. J Urol. 1972; 107(6):1008–1016. [PubMed: 4113688]
7. Hazle JD, Diederich CJ, Kangasniemi M, et al. MRI-guided thermal therapy of transplanted tumors in the canine prostate using a directional transurethral ultrasound applicator. J Magn Reson Imaging. 2002; 15(4):409–17. [PubMed: 11948830]
8. Diederich C, Burdette E. Transurethral ultrasound array for prostate thermal therapy: initial studies. IEEE Trans Ultrason Ferroelect Frequ Contr. 1996; 43:1011–1022.
9. Ross AB, Diederich CJ, Nau WH, et al. Curvilinear transurethral ultrasound applicator for selective prostate thermal therapy. Med Phys. 2005; 32(6):1555–1565. [PubMed: 16013714]
10. Ross AB, Diederich CJ, Nau WH, et al. Highly Directional Transurethral Ultrasound Applicators with Rotational Control for MRI Guided Prostatic Thermal Therapy. Phys Med Biol. 2004; 49(1): 189–204. [PubMed: 15083666]
11. Wootton JH, Ross AB, Diederich CJ. Prostate thermal therapy with high intensity transurethral ultrasound: the impact of pelvic bone heating on treatment delivery. Int J Hyperthermia. 2007; 23(8):609–622. [PubMed: 18097849]
12. Pauly KB, Diederich CJ, Rieke V, et al. Magnetic resonance-guided high-intensity ultrasound ablation of the prostate. Top Magn Reson Imaging. 2006; 17(3):195–207. [PubMed: 17414077]
13. Diederich CJ, Nau WH, Ross AB, et al. Catheter-based ultrasound applicators for selective thermal ablation: progress towards MRI-guided applications in prostate. Int J Hyperthermia. 2004; 20(7): 739–756. [PubMed: 15675669]
14. Diederich, C.; Rieke, V.; Nau, W., et al. Medical Physics. New York: 2010. Transurethral ultrasound applicators with dynamic multi-sector control for prostate thermal therapy: emph TYPE=“ 1”> In vivo evaluation under MR …. …
15. Chopra R, Burtnyk M, N'djin WA, et al. MRI-controlled transurethral ultrasound therapy for localised prostate cancer. Int J Hyperthermia. 2010; 26(8):804–821. [PubMed: 21043572]
16. Siddiqui K, Chopra R, Vedula S, et al. MRI-guided transurethral ultrasound therapy of the prostate gland using real-time thermal mapping: initial studies. Urology. 2010; 76(6):1506–1511. [PubMed: 20709381]
17. Nau WH, Diederich CJ, Burdette EC. Evaluation of multielement catheter-cooled interstitial ultrasound applicators for high-temperature thermal therapy. Med Phys. 2001; 28(7):1525–1534. [PubMed: 11488586]

18. Diederich CJ, Stafford RJ, Nau WH, et al. Transurethral ultrasound applicators with directional heating patterns for prostate thermal therapy: in vivo evaluation using magnetic resonance thermometry. Med Phys. 2004; 31(2):405–413. [PubMed: 15000627]
19. Diederich CJ, Nau WH, Stauffer PR. Ultrasound applicators for interstitial thermal coagulation. IEEE Trans Ultrason Ferroelectr Freq Control (USA). 1999; 46(5):1218–1228.
20. Ross AB, Diederich CJ, Sommer G, et al. Highly directional transurethral ultrasound applicators with rotational control for MRI-guided prostatic thermal therapy. Phys Med Biol. 2004; 49(2): 189–204. [PubMed: 15083666]
21. Nau WH, Diederich CJ, Ross AB, et al. MRI-guided interstitial ultrasound thermal therapy of the prostate: a feasibility study in the canine model. Med Phys. 2005; 32(3):733–743. [PubMed: 15839345]
22. Diederich CJ, Nau WH, Burdette EC, et al. Combination of transurethral and interstitial ultrasound applicators for high-temperature prostate thermal therapy. Int J Hyperthermia. 2000; 16(5):385–403. [PubMed: 11001573]
23. Diederich CJ. Interstitial ultrasound applicators are practical from an engineering perspective for treating large tumours. Int J Hyperthermia. 1996; 12(2):305–306. letter; comment. [PubMed: 8926398]
24. Kinsey AM, Diederich CJ, Tyreus PD, et al. Multisectored interstitial ultrasound applicators for dynamic angular control of thermal therapy. Med Phys. 2006; 33(5):1352–1363. [PubMed: 16752571]
25. Chen J, Daniel BL, Diederich CJ, et al. Monitoring prostate thermal therapy with diffusion-weighted MRI. Magn Reson Med. 2008; 59(6):1365–1372. [PubMed: 18506801]
26. Rieke V, Kinsey AM, Ross AB, et al. Referenceless MR thermometry for monitoring thermal ablation in the prostate. IEEE Trans Med Imaging. 2007; 26(6):813–821. [PubMed: 17679332]
27. Rieke V, Vigen KK, Sommer G, et al. Referenceless PRF shift thermometry. Magn Reson Med. 2004; 51(6):1223–1231. [PubMed: 15170843]
28. Pauly KB, Diederich CJ, Rieke V, et al. Magnetic resonance-guided high-intensity ultrasound ablation of the prostate. Top Magn Reson Imaging. 2006; 17(3):195–207. [PubMed: 17414077]
29. Holbrook, A.; Santos, J.; Kaye, E. Magnetic Resonance in Medicine. Wiley Online Library; 2010. Real-time MR thermometry for monitoring HIFU ablations of the liver - Holbrook - 2009. Magnetic …
30. Bouley, DM.; Daniel, B.; Butts Pauly, K., et al. Proceedings of SPIE. Vol. 6440. SPIE; 2007. p. 644006-12.644006
31. Bouley D, Sommer G, Kaye E, et al. 173. Evaluation of thermal and cryo lesions by diffusion-weighted MRI. Cryobiology. 2006
32. Daniel B, Bouley D, Sommer G, et al. Evaluation of thermal and cryo lesions by diffusion-weighted MRI. 2007
33. Kinsey AM, Diederich CJ, Rieke V, et al. Transurethral ultrasound applicators with dynamic multi-sector control for prostate thermal therapy: in vivo evaluation under MR guidance. Med Phys. 2008; 35(5):2081–2093. [PubMed: 18561684]
34. Diederich CJ, Nau WH, Burdette EC, et al. Combination of transurethral and interstitial ultrasound applicators for high-temperature prostate thermal therapy. Int J Hyperthermia. 2000; 16(5):385–403. [PubMed: 11001573]
35. Planey C, Santos J, Diederich C, et al. Multislice Treatment Planning and Control for Real Time MR-Guided Prostate Ablation with Transurethral Multisectored Ultrasound Applicators 2AD.
36. Coad JE, Kosari K, Humar A, et al. Radiofrequency ablation causes “thermal fixation” of hepatocellular carcinoma: a post-liver transplant histopathologic study. Clin Transplant. 2003; 17(4):377–384. [PubMed: 12868996]
37. Kincaide LF, Sanghvi NT, Cummings O, et al. Noninvasive ultrasonic subtotal ablation of the prostate in dogs. Am J Vet Res. 1996; 57(8):1225–1227. [PubMed: 8836379]
38. Gelet A, Chapelon JY, Margonari J, et al. Prostatic tissue destruction by high-intensity focused ultrasound: experimentation on canine prostate. J Endourol. 1993; 7(3):249–253. [PubMed: 8358423]

39. Mynderse LA, Larson B, Huidobro C, et al. Characterizing TUNA ablative treatments of the prostate for benign hyperplasia with gadolinium-enhanced magnetic resonance imaging. J Endourol. 2007; 21(11):1361–1366. [PubMed: 18042031]
40. Ghanouni P, Gill H, Kaye E, et al. MR Imaging–guided Cryoablation for the Treatment of Benign Prostatic Hyperplasia. Journal of Vascular and …. 2011
41. Bott SRJ, Ahmed HU, Hindley RG, et al. The index lesion and focal therapy: an analysis of the pathological characteristics of prostate cancer. BJU Int. 2010; 106(11):1607–1611. [PubMed: 20553262]
42. Eggener SE, Scardino PT, Carroll PR, et al. Focal therapy for localized prostate cancer: a critical appraisal of rationale and modalities. J Urol. 2007; 178(6):2260–2267. [PubMed: 17936815]
43. Bill-Axelson A, Holmberg L, Ruutu M, et al. Radical prostatectomy versus watchful waiting in early prostate cancer. N Engl J Med. 2011; 364(18):1708–1717. [PubMed: 21542742]
44. Ip S, Dahabreh I, Chung M, et al. Ongoing Randomized Studies Comparing Observational Management Strategies With Active Treatment Strategies for the Treatment of Clinically Localized Disease. 2011
45. Weinreb JC, Blume JD, Coakley FV, et al. Prostate cancer: sextant localization at MR imaging and MR spectroscopic imaging before prostatectomy--results of ACRIN prospective multi-institutional clinicopathologic study. Radiology. 2009; 251(1):122–133. [PubMed: 19332850]
46. Langer DL, van der Kwast TH, Evans AJ, et al. Prostate cancer detection with multi-parametric MRI: logistic regression analysis of quantitative T2, diffusion-weighted imaging, and dynamic contrast-enhanced MRI. J Magn Reson Imaging. 2009; 30(2):327–334. [PubMed: 19629981]
47. McNeal JE. Cancer volume and site of origin of adenocarcinoma in the prostate: relationship to local and distant spread. Hum Pathol. 1992; 23(3):258–266. [PubMed: 1555836]
48. Madersbacher S, Schatzl G, Djavan B, et al. Long-term outcome of transrectal high-intensity focused ultrasound therapy for benign prostatic hyperplasia. Eur Urol. 2000; 37(6):687–694. [PubMed: 10828669]
49. Rouvière O, Souchon R, Salomir R, et al. Transrectal high-intensity focused ultrasound ablation of prostate cancer: effective treatment requiring accurate imaging. Eur J Radiol. 2007; 63(3):317–327. [PubMed: 17689218]

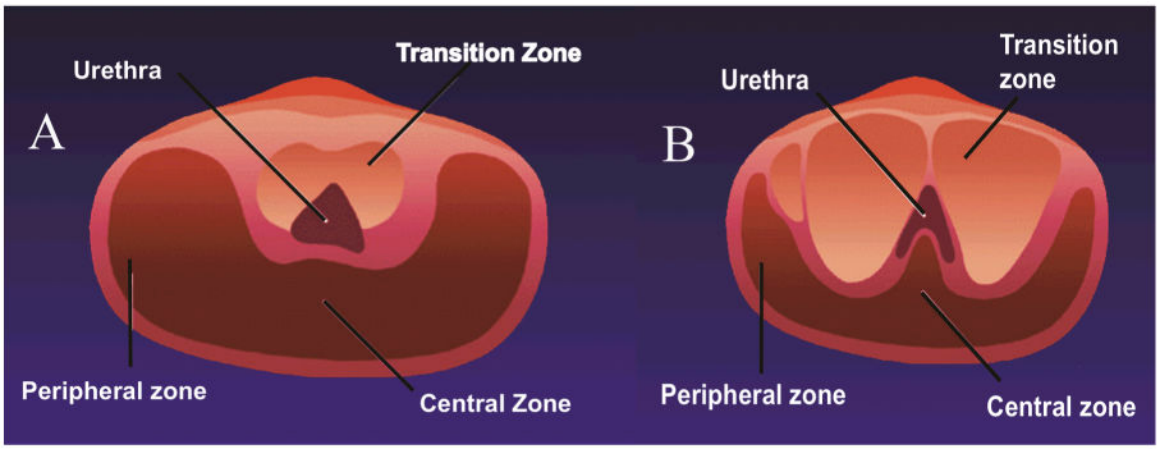

Figure 1.

Common appearance of benign prostatic hyperplasia (BPH) shown diagramatically in axial plane through mid gland. A) in the normal prostate, the transition zone lobes abut the prostatic urethra at its anterolateral aspect. Other major glandular regions (peripheral and central zones) are also present as indicated, at this level. B) in a typical prostate involved with moderate BPH, the enlarged transition zone lobes compress the prostatic urethra significantly.

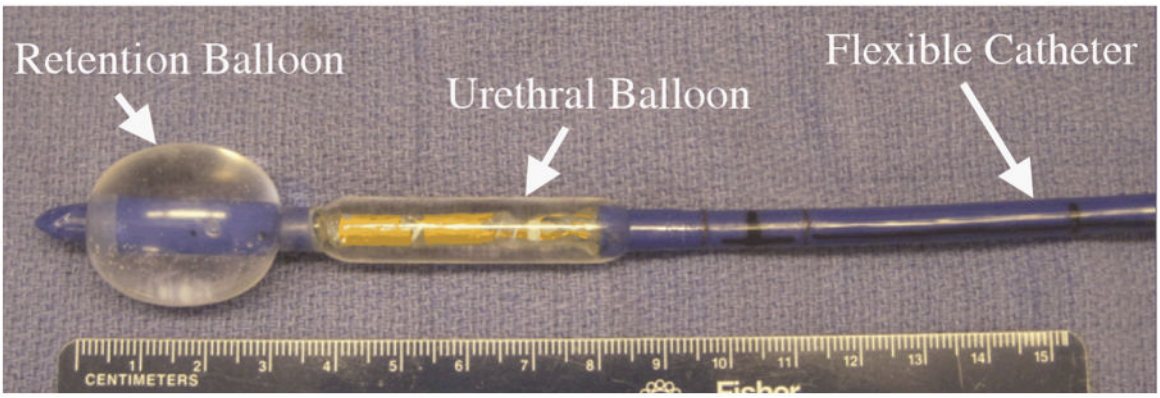

Figure 2.

Transurethral catheter designed to have capability for ablation of human BPH. Major features include: the retention balloon which is filled with a 1% solution of gadolinium contrast agent after catheter insertion, to maintain positioning of the device within the prostatic urethra and MRI visibility; the urethral balloon which is inflated within the prostatic urethra and through which water circulates during ablation; and the flexible catheter containing electronic connections. Within the urethral balloon are the transducers, two 10 mm long cylindrical transducers with dual 120 degree active sectors.

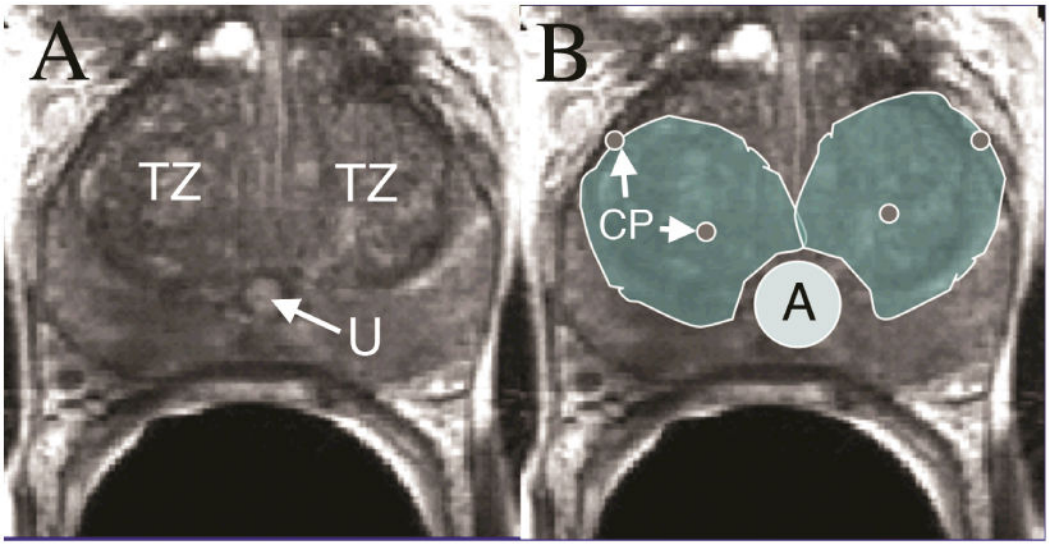

Figure 3.

Treatment simulation of human BPH using MRI and RThawk treatment control software A) T2-weighted axial image through the mid-portion of a human prostate with BPH and enlarged transition zones (TZ) anterolateral to the urethra (U). B) BPH treatment plan with targeted TZ tissue indicated by green regions, and control points for therapy delivery monitored by MRTI indicated by 4 small gray circles (CP). Applicator (A) is present in the urethra.

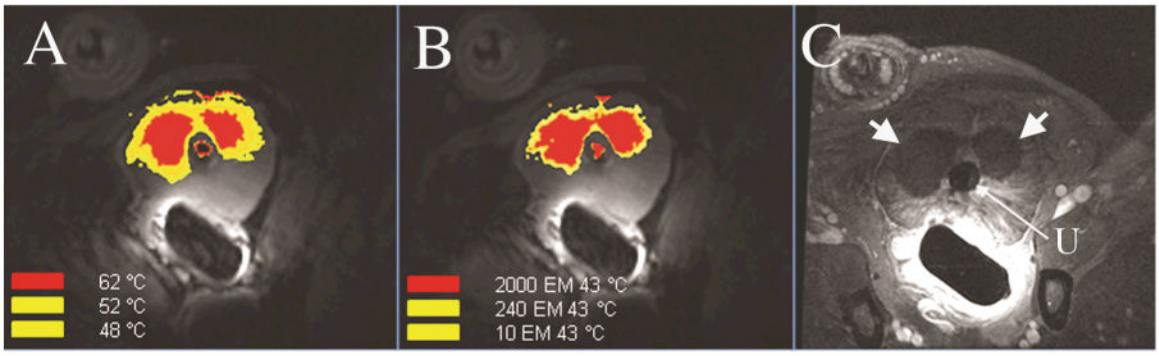

Figure 4.

MR Images obtained during acute study of ablation of a canine prostate in vivo. A) MRTI showing the spatial distribution of maximum temperatures recorded during the ablation B) MRTI map showing thermal dosimetry in equivalent minutes at 43°C during the ablation C) Contrast enhanced T1-weighted image obtained following the ablation shows two anterolateral regions in the prostate (large arrows) which have been ablated and appear dark due to lack of blood flow. The applicator in the prostatic urethra (U) is visible in this image. In A) and B), the applicator contains some artifactual color due to circulating water in the urethral cooling balloon.

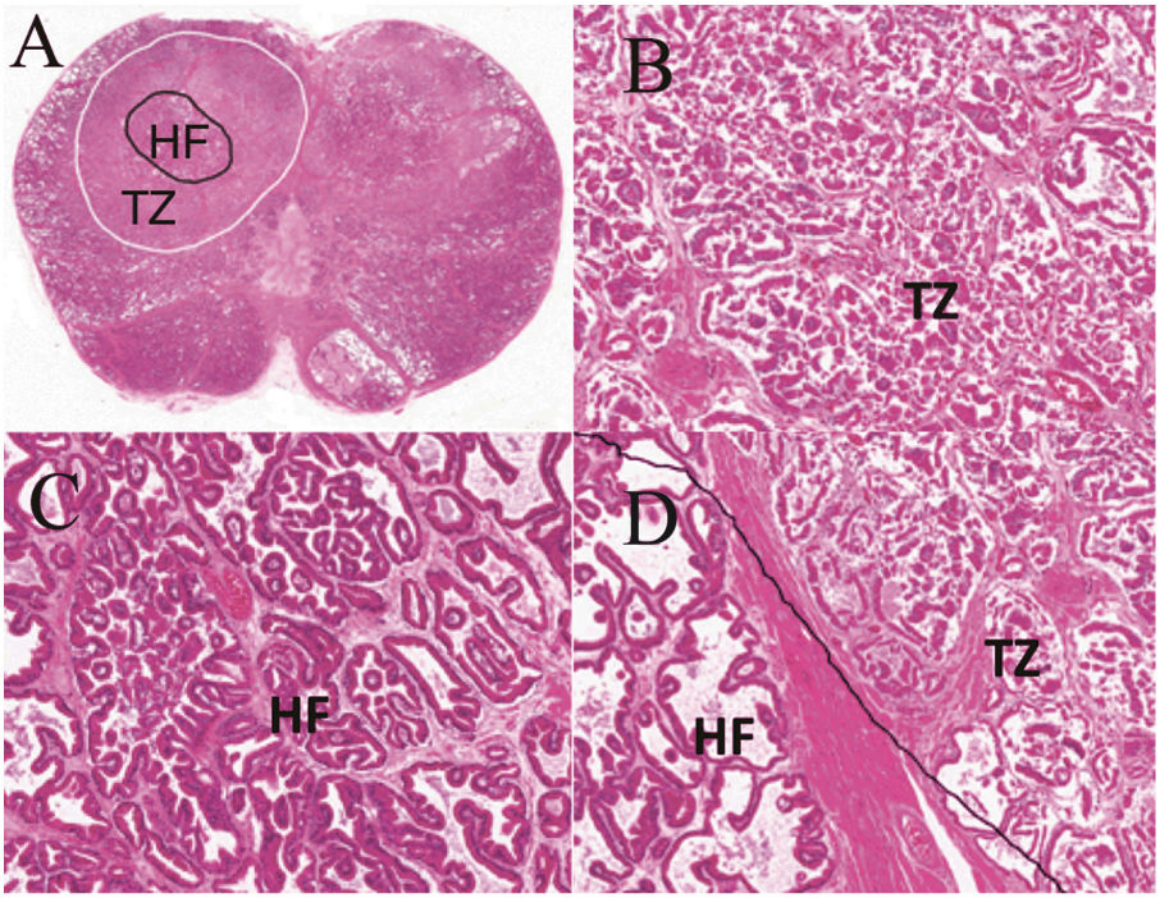

Figure 5.

Histologic analysis of the prostate ablated in the acute study illustrated in Figure 4. H and E stained images at the illustrated ablation level are shown: A) Whole mount section of the prostate demonstrates 2 prominent regions of ablation anterolaterally corresponding to the nonperfused regions seen in Figure 4C. The ablated region contains 2 distinct regions, a central heat-fixed region (HF) and a peripheral transition zone (TZ). The markedly disrupted tissue architecture of the TZ (B) contrasts strikingly with the near normal appearance of the heat-fixed region (C) which was rapidly heated to a higher temperature than the TZ. The boundary between the HF and TZ zones is abrupt and distinct, as shown in (D).

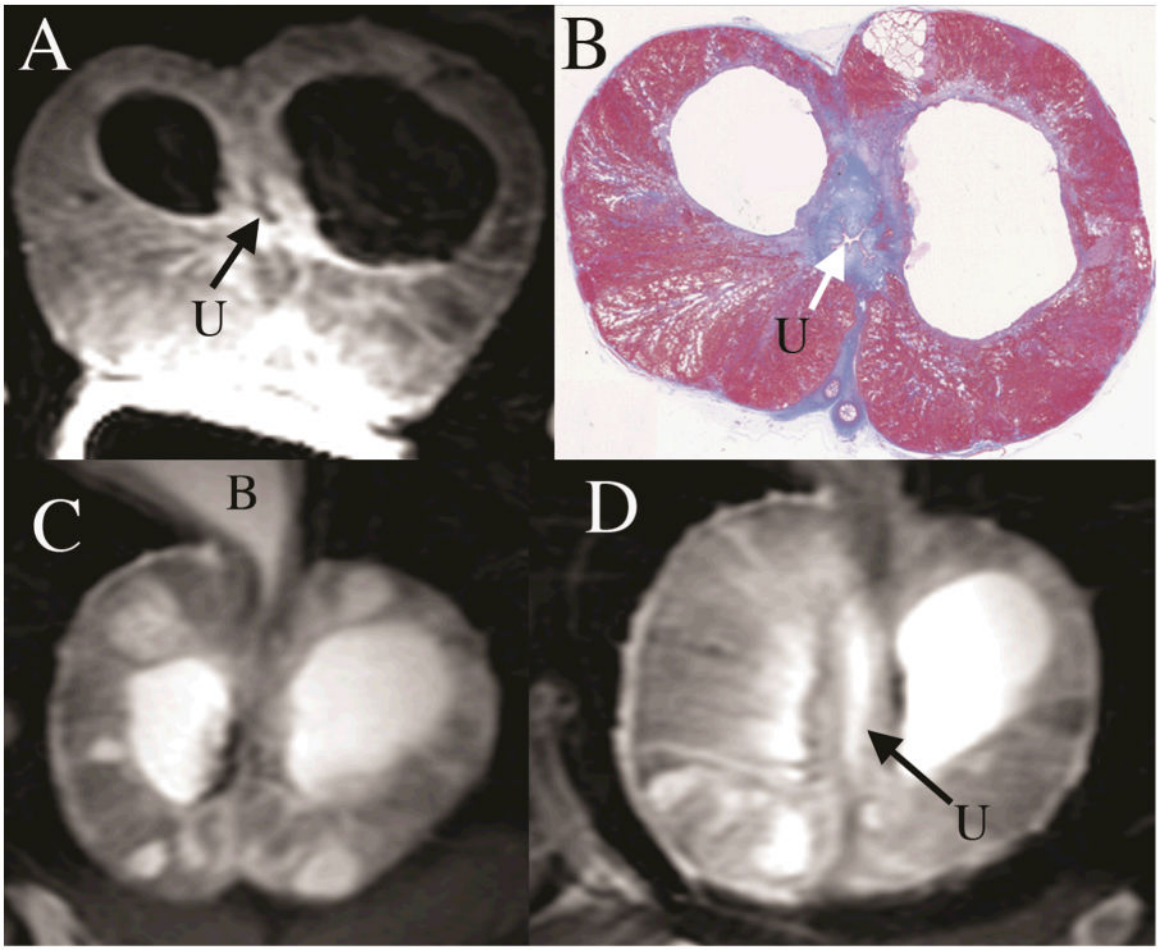

Figure 6.

Images of enlarged canine prostate involved with extensive BPH, with two regions of ablation created under MRI guidance anterolaterally, and studied 31 days later (chronic study). A) Contrast enhanced T1-weighted image shows 2 large avascular regions anterolaterally to the urethra (U) with some enhancement at margins. B) Correlative trichrome stained histologic image shows the two large cystic spaces with some collagenous tissue at their margins. There is complete preservation of the prostatic urethra (U). C) and D) Two T2-weighted images show both the extensive cystic change throughout the gland due to BPH, and the two large residual cystic spaces on either side of the intact urethra (U). In C), the bladder neck (B) is visible cranial to the enlarged prostate gland.

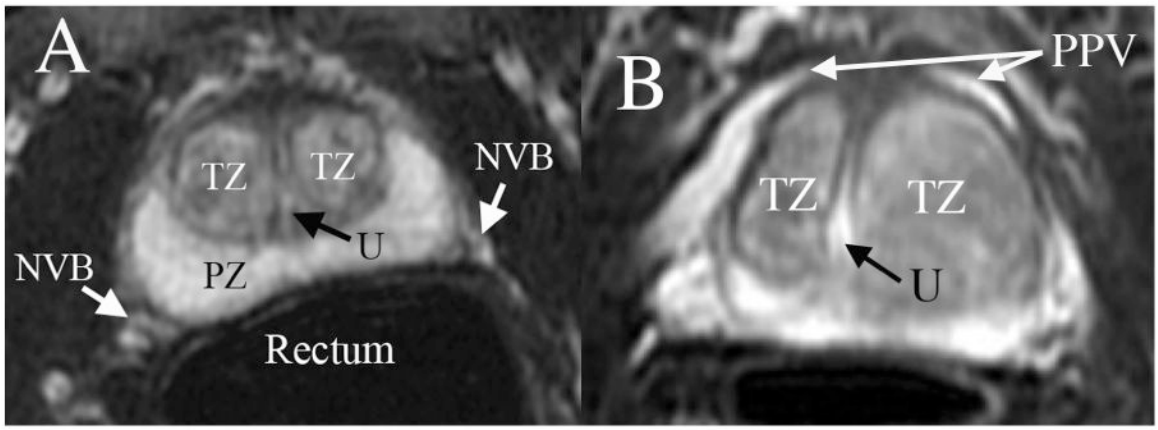

Figure 7.

Two examples of human BPH as depicted in fat suppressed axial T2-weighted MRI through the midportions of the prostate gland A) MRI of a patient with moderate BPH. The two transition zone (TZ) lobes are seen anterolateral to the prostatic urethra (U), and there is clear differentiation of the TZ from the more posterior peripheral zone (PZ), which has a higher signal intensity. Critical structures at risk for damage during ablation include the bilateral neurovascular bundles (NVB), and the rectum. B) Prostate MRI of a patient with more severe BPH shows assymetrical enlargement of TZ lobes, with the left being significantly larger. Compressed urethra (U) is seen between enlarged TZ lobes. The anterolateral aspects of the prostate are surrounded by slow flowing blood in the periprostatic venous plexus (PPV)